Error Mechanism Modeling and Prediction of Current Transformers under Dynamic Influencing Factors

Yongda Yang[1], Wei Qiu[1], Yao Zhang[1], Yixi Zou[1], He Yin[1], Wenxuan Yao[1]

[1]*College of Electrical and Information Engineering, Hunan University,* Changsha, China
qiu@hnu.edu.cn, qiuwei@hnu.edu.cn, wenxuanyao@hnu.edu.cn, heyin@hnu.edu.cn

***Abstract*—Current transformers are pivotal for energy metering and protection in distribution networks, with measurement accuracy directly affecting the economic interests of utilities and end users. To ensure metering system reliability, this study systematically examines error sources in current transformers across diverse operating conditions, elucidating the influence mechanisms of primary current temperature, magnitude, frequency, and ambient electromagnetic fields. Specifically, a validated multiphysics simulation model is developed to quantify the impacts of these coupled fields on measurement errors. In addition, a physics-guided deep neural network regression model is constructed to predict multi-variable errors of current transformers under dynamic operating conditions. By integrating multiple physically meaningful input variables, the model accurately predicts both ratio error and phase error, thereby supporting condition assessment and online monitoring of metering devices. Simulation results indicate that the proposed method achieves a threefold improvement over recently developed approaches, with a practical efficiency gain far exceeding seventy times.**

Keywords—Current transformer, error mechanism, metering, error analysis, prediction model.

I. INTRODUCTION

In recent years, metering current transformers have been extensively deployed in distribution networks, with current measurement capabilities ranging from DC to several kiloamperes. As fundamental devices for energy billing, their measurement accuracy directly impacts refined line loss management and the economic interests of both power suppliers and consumers [1]. Taking a traction substation as an example, a current transformer with a rated ratio of 400/5 A was found to under-record 27.65 kW·h within 8 minutes, leading to an annual energy shortfall of 1.68×10^4 kW·h [2]. At an industrial electricity price of 1.80 RMB/kW·h, this results in a reduction of approximately 30,000 RMB in annual billing revenue, causing significant economic losses to the power supply enterprise. Therefore, it is essential to elucidate the influence mechanisms of factors such as temperature [3], enabling operation and maintenance personnel to assess equipment conditions in a timely manner, prevent metering failures, ensure accurate energy settlement, and reduce economic losses for both supply and consumption parties [4].

This work was supported in part by the National Natural Science Foundation of China under Grant 52307093, and in part by Hunan Provincial Natural Science Foundation of China under Grant 2025JJ40045, and in part by National Natural Science Foundation of China under Grant 52407095, and in part by the Natural Science Foundation of Hunan Province under Grant 2025JJ60373.

In practical operation, metering current transformers are subjected to various complex scenarios, including single-phase grounding, DC bias [5], moisture from rain, extreme temperatures, and frequency deviations [6]. Each of these conditions imposes unique stresses on the device and can significantly affect measurement accuracy [7].

To address these challenges, developing computer simulation models based on practical experience to characterize current transformer behavior represents a cost-effective solution. However, conventional modeling approaches primarily rely on circuit theory, which involves inherent uncertainties in parameter determination, requires simplified assumptions, and often neglects multiple variables, ultimately limiting accuracy.

To overcome these limitations, this study focuses on investigating the effects of dynamic factors such as the amplitude, frequency, temperature, electric field, and magnetic field of the primary current. The primary contributions of this work are outlined as follows:

1) A finite-element current-transformer model is established to analyze how diverse external factors affect metering error and to reveal their variation trends.

2) A physics-guided deep neural network-based prediction model for multi-variable errors in current transformers (CT-ErrorNet) is constructed, integrating the error-mechanism analysis and finite-element simulations to enable extrapolation under limited test conditions and to improve simulation efficiency.

II. THEORETICAL ANALYSIS OF CURRENT TRANSFORMER

A. Principle Analysis of Primary Current Amplitude Affecting Error

Upon completion of standard demagnetization procedures, the error of a current transformer is primarily governed by the primary current, which determines the operating point on the core's magnetization curve. The magnetization curve serves as a critical indicator of current transformer performance, wherein the incremental permeability of the core, $\mu = B/H$, is not constant.

Under normal operating conditions, the magnetic flux density in the core remains low, and the current transformer operates within the unsaturated zone. At very low primary currents, the operating point lies in the initial unsaturated segment where permeability is low, requiring higher excitation ampere-turns and leading to increased measurement errors. When the primary current approaches the rated value, the operating point shifts to the medium-flux region, where higher permeability reduces excitation requirements and minimizes errors. If the primary current

979-8-3315-8138-1

exceeds the rated value, the core begins to saturate, causing a rapid increase in excitation current and required ampere-turns, which in turn significantly amplifies the current transformer error [8]. In accordance with JJG 313-2010, the permissible error limits are stricter for the 20%-120% rated current range compared to the 1%-5% range.

Therefore, to achieve minimized measurement error, the electric energy metering system should be designed to maintain the current in the measured circuit within 60% to 100% of the transformer's rated current.

B. Principle Analysis of Frequency Influence Error

Changes in frequency modify the permeability, eddy current loss, and hysteresis characteristics of the core, and thereby affect the excitation current and the measurement error of the current transformer [9].

Let the total resistance of the secondary circuit of the current transformer be R_s, and the total inductance be L_s. The voltage drop generated when the secondary current I_2 of the current transformer passes through the secondary total impedance is equal to the induced potential E_2 of the secondary coil, that is:

$$E_2 = I_2 Z_2 = I_2\sqrt{R_s^2 + (2\pi f L_s)^2} \tag{1}$$

where Z_2 denotes the secondary impedance, f denotes the frequency. According to the law of electromagnetic induction:

$$E_2 = 4.44 f W B_m S \propto f B_m \tag{2}$$

where W denotes the number of turns of the coil, B_m denotes the maximum value of magnetic flux density, S denotes the effective cross-sectional area of iron core. that is:

$$I_2\sqrt{R_s^2 + (2\pi f L_s)^2} \propto f B_m \tag{3}$$

It can be seen from (3) that when the frequency increases, the magnetic flux density in the core decreases, so the excitation current and excitation ampere-turns also decrease. This reduces both ratio error and phase error and improves the accuracy of the current transformer.

C. Principle Analysis of Temperature Influence Error

Variations in temperature can lead to changes in the structural parameters of the iron core, the total impedance of the secondary circuit, and the permeability, thereby affecting the error of the current transformer [10].

Permeability is a physical quantity that characterizes the magnetic properties of a magnetic medium and is related to material attributes. Common core materials for metering current transformers include silicon steel sheets, iron-nickel alloys, and amorphous alloys. The permeability of silicon steel sheets and iron-nickel alloys increases with rising temperature, with silicon steel sheets experiencing a permeability change of approximately 0.012% per 1 °C change, and iron-nickel alloys about 0.2% per 1 °C change. In contrast, for high-precision silicon steel sheets with high silicon content, permeability decreases as temperature increases.

Thus, if the permeability of the core material decreases with increasing temperature, the error will correspondingly increase.

D. Principle Analysis of Magnetic Field Influence Error

When a current transformer is situated near current-carrying conductors, it operates within an external magnetic field. A portion of the magnetic flux generated by these adjacent conductors links with the secondary winding of the transformer. As the current varies over time, this flux induces an electromotive force (EMF) in the secondary winding, thereby generating additional currents in the secondary circuit [11].

Schematic diagram of the equivalent mutual coupling circuit under the influence of an external magnetic field is presented in Fig. 1. In Fig. 1, M_{13} represents the mutual inductance between the external current-carrying conductor and the primary winding, M_{23} denotes the mutual inductance between the external conductor and the secondary winding, L_3 is the self-inductance of the external conductor, r_3 represents the resistance of the external conductor, U_3 stands for the terminal voltage of the external conductor.

The voltage equations for the primary and secondary circuits in Fig. 1 can be expressed as follows:

$$(r_1 + j\omega L_1)\dot{I}_1 + j\omega M_{12}\dot{I}_2 + j\omega M_{13}\dot{I}_3 = \dot{U}_1 \tag{4}$$

$$\mathrm{j}\omega M_{12}\dot{I}_1 + (r_2 + \mathrm{j}\omega L_2 + Z_\mathrm{L})\dot{I}_2 + \mathrm{j}\omega M_{23}\dot{I}_3 = 0 \tag{5}$$

where I_3 represents the current of the external current-carrying conductor, referred to the secondary side, M_{12} denotes the mutual inductance between the primary and secondary windings. r_1, L_1, U_1, and I_1 represent the resistance, inductance, voltage, and current of the primary winding, all referred to the secondary side. K_{23} is the turns ratio between the secondary winding and the external current-carrying conductor.

By combining (4) and (5) and solving for the secondary current under the influence of the external magnetic field, the error can be expressed as:

$$\varepsilon_{ic} = \frac{-\dot{I}_2 - \dot{I}_1'}{\dot{I}_1'} = \frac{N_2}{N_1} \cdot \frac{j\omega\ {}_{12}\dot{I}_1 + j\omega M_{23}\dot{I}_3}{(r_2 + j\omega L_2 + Z_L)\dot{I}_1} - 1 \tag{6}$$

$$\varepsilon_{ic} = \frac{-\dot{I}_2 - \dot{I}_1'}{\dot{I}_1'} = -\left(\frac{N_2}{N_1}\right)^2 \cdot \frac{\dot{U}_1 - j\omega M_{13}\dot{I}_3 - (r_1 + j\omega L_1)\dot{I}_1}{j\omega\ {}_{12}\dot{I}_1} - 1 \tag{7}$$

Therefore, it can be concluded that the physical quantities related to the magnetic field are I_3, M_{13}, and M_{23}. I_3 determines the magnitude and direction of the magnetic field, while M_{13} and M_{23} are determined by the spatial relationship between the external current-carrying conductor and the current transformer.

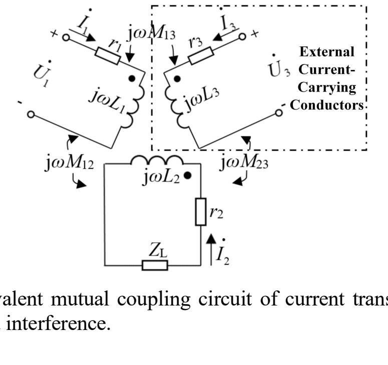

Fig. 1. Equivalent mutual coupling circuit of current transformer under magnetic field interference.

979-8-3315-8138-1

E. Principle Analysis of Electric Field Influence Error

When the external factor is an electric field, the electric field itself does not directly cause changes in metering error. Maxwell's equations reveal that a space filled with a changing electric field is simultaneously permeated by a changing magnetic field [12].

The magnitude of the induced magnetic field is directly dictated by the frequency of the electric field. This study focuses on electromagnetic fields at 50 Hz, which falls within the extremely low-frequency range.

Consequently, the magnetic flux density induced solely by the power-frequency electric field is negligible.

III. Simulation Analysis

A. Model Establishment

A simulation model was constructed based on a small current transformer with a rated transformation ratio of 1:1000. The model is composed of a primary winding, a secondary winding, and a magnetic core, and its rendering in Maxwell 3D is illustrated in Fig. 2.

B. Error Analysis of Amplitude and Frequency

To quantitatively assess how the primary-current amplitude and frequency affect the measurement error of a current transformer, AC currents of varying amplitudes and frequencies are applied to the primary winding to obtain secondary currents at different operating points, and the corresponding errors are calculated from the simulation results. The results are illustrated in Fig. 3.

The current amplitude is swept from 5 A to 720 A using twelve levels 5 A, 10 A, 30 A, 40 A, 50 A, 60 A, 90 A, 120 A, 300 A, 480 A, 600 A and 720 A. At each level a 50 Hz sinusoidal current is applied and the steady-state primary and secondary currents are used to calculate the ratio and phase errors. As the primary current increases, the ratio error first decreases to a minimum of 0.0499% at 120 A and then increases, while the phase error is relatively small only at 120 A and 300 A and shows an overall increasing trend, as illustrated in Fig. 3(a).

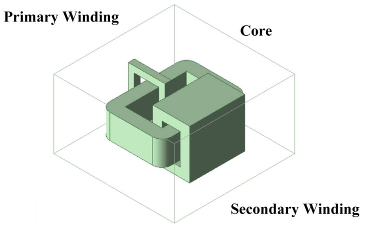

Fig. 2. CT model in Maxwell 3D.

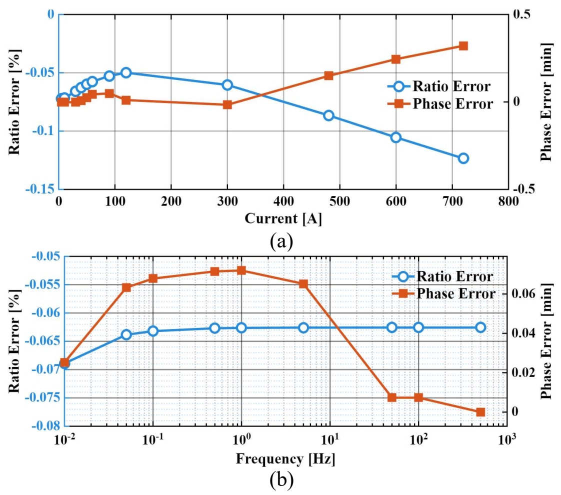

Fig. 3. Simulation results for amplitude and frequency, (a) trend of error with amplitude, (b) trend of error with frequency.

In the frequency impact test, the frequency is swept from 0.01 Hz to 500 Hz while the primary current amplitude is fixed at 40 A. At each frequency point 0.01 Hz, 0.05 Hz, 0.1 Hz, 0.5 Hz, 1 Hz, 2 Hz, 5 Hz, 50 Hz, 100 Hz and 500 Hz, a sinusoidal current of that frequency is applied on the primary side, and the steady-state primary and secondary currents from the simulations are used to compute the ratio and phase errors. The ratio error gradually decreases with increasing frequency and then stabilizes, whereas the phase error increases, reaches a maximum of 0.0719 min at 1 Hz, and then gradually decreases, as shown in Fig. 3(b).

C. Temperature Error Analysis

To evaluate temperature effects on the measurement error of a current transformer, the ambient temperature is varied and the corresponding secondary currents and errors are obtained. Because the simulation environment cannot directly impose a temperature field, temperature influence is represented by adjusting temperature-dependent material properties, including winding conductivity, core conductivity and the magnetic characteristics of the core.

For the magnetic core, a family of B-H curves is measured from -40 °C to 80 °C and imported into Maxwell as a temperature-indexed material data set, as shown in Fig. 4. During simulation, the solver interpolates between the curves according to the specified ambient temperature so that both incremental permeability and saturation flux density vary with temperature, and the resulting shift of the operating point and onset of saturation are reflected in the calculated excitation current and error.

The eddy current loss coefficient, permeability and electrical conductivity all decrease with temperature, while the hysteresis loss coefficient increases. By updating these parameters at each temperature level and using the corresponding material data in the finite-element model, the influence of ambient temperature on metering error is simulated without directly applying a temperature field.

In the temperature-impact study, the ambient temperature is set to -40, -25, -10, 0, 20, 40, 60 and 80 °C. After updating the temperature-dependent data and rerunning the simulations, the error variations shown in Fig. 5 are obtained. The absolute value of the ratio error increases with temperature, with a maximum change of 0.0306%, and the phase error also increases with temperature.

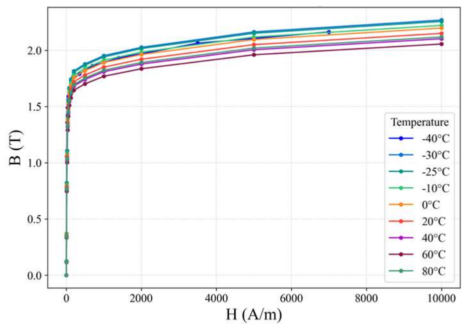

Fig. 4. B-H curves at various temperatures.

979-8-3315-8138-1

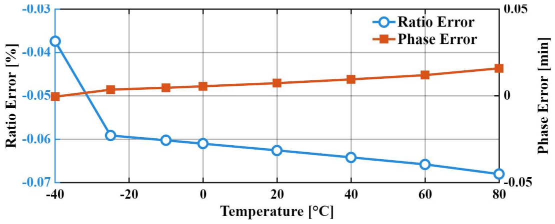

Fig. 5. Simulation results for temperature.

D. Error Analysis of Magnetic Field

In practical applications, external current-carrying conductors may be straight wires or coils, but their magnetic fields can all be analyzed by the Biot-Savart law. In this study, two parallel square coils with the same current direction are used as representative external conductors, as shown in Fig. 6(a). The center of the current transformer's operating area is taken as the reference point. Under power-frequency excitation, coil currents of 100 A, 200 A, 400 A, 600 A, 800 A, 1000 A and 1200 A generate magnetic flux densities of 111.77 μT, 223.61 μT, 444.6 μT, 667.16 μT, 888.9 μT, 1110.89 μT and 1333.07 μT, demonstrating that the magnetic-field strength is directly proportional to the coil current. Therefore, studying the relationship between magnetic flux density and error is equivalent to studying the relationship between external current and error. Considering the influence of adjacent phase conductors, the current transformer is placed with its winding-coil axis parallel to the y-axis. The calculated ratio and phase errors for different external currents are shown in Fig. 7, and both errors increase with magnetic flux density.

E. Error Analysis of Electric Field

The electric-field simulation model consists of two parallel plates. Applying an AC voltage to the plates forms a uniform field between them, as shown in Fig. 6(b).

When the plate voltages are 10 kV, 20 kV, 40 kV, 60 kV, 80 kV and 96 kV, the electric-field intensities at the center of the current transformer are 11,690.6 V/m, 29,081.3 V/m, 46,762.5 V/m, 70,143.8 V/m, 93,525.0 V/m and 112,230.0 V/m. This shows that the electric-field intensity is directly proportional to the plate voltage, so studying the relationship between electric-field intensity and error is equivalent to studying the relationship between plate voltage and error.

Since the electric field exerts its influence through the induction of a magnetic field, the simulation approach aligns with that used for magnetic fields. Given that the induced magnetic field intensity is relatively small, the calculated results of ratio error and phase error variations with plate voltage are presented in Fig. 8.

As can be seen from Fig. 8, the ratio error and phase error remain almost constant as the plate voltage increases.

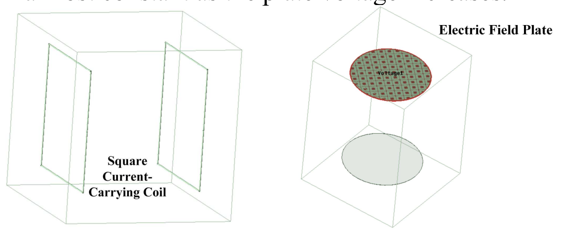

(a) (b)

Fig. 6. Square current-carrying coil and electrode plates, (a) magnetic Field, (b) electric Field.

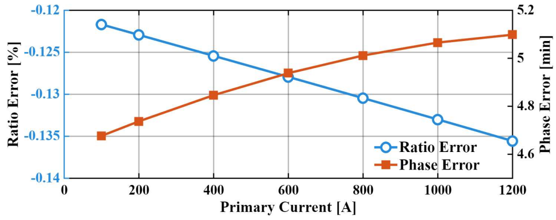

Fig. 7. Simulation results for magnetic field.

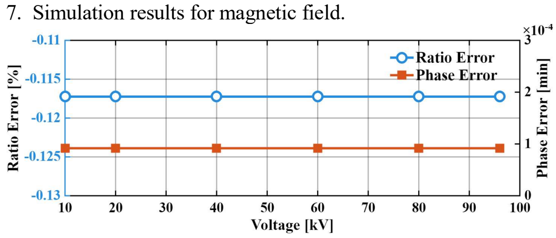

Fig. 8. Simulation results for electric field.

IV. Prediction Model

To characterize the impact of five variables on measurement errors, exhaustive testing at 10 levels per variable would require 100000 tests, which is impractical. Instead, this study develops CT-ErrorNet, a physics-guided fully connected deep neural network for predicting multi-variable errors in current transformers. CT-ErrorNet takes five standardized inputs, primary current amplitude, frequency, temperature, electric field intensity and magnetic flux density, and uses a compact multilayer perceptron with three hidden layers of 64, 32 and 16 neurons with ReLU activations and a linear output neuron to predict ratio error and phase error. By learning and interpolating the error laws revealed by finite-element simulations, the model enables rapid and accurate prediction of metering errors over the full parameter space.

Full-range error predictions for pairwise interdependent variables are shown in Fig. 9. CT-ErrorNet reproduces relationships that previously required complex formulas or finite-element simulations. Once trained, it performs predictions within milliseconds, replacing simulations or experiments that would otherwise take hours or days. Although it is a relatively compact network, its nonlinear structure is sufficient to capture the main working mechanisms of the current transformer and to interpolate under variable combinations not present in the training data, generating continuous multidimensional error surfaces.

To validate the model, three sets of prediction data were selected as test points in Fig. 9. Unspecified test conditions were fixed at temperature 20 °C, current 40 A, frequency 50 Hz and electromagnetic field strength 0. The predictions were compared with traditional methods and measurements, as listed in Table I. The relative ratio and phase errors are derived based on Table I, as demonstrated in Fig. 10. It can be found that the prediction error of CT-ErrorNet is lower than that of polynomial regression and more than three times better than traditional methods, confirming its effectiveness.

The Maxwell simulation required about 654 seconds to compute these three data points, whereas CT-ErrorNet produced the corresponding results in less than one seventeenth of that time. When electromagnetic field coupling is included and the model complexity increases, the simulation time for one dataset can exceed that of CT-ErrorNet by more than four orders of magnitude,

979-8-3315-8138-1

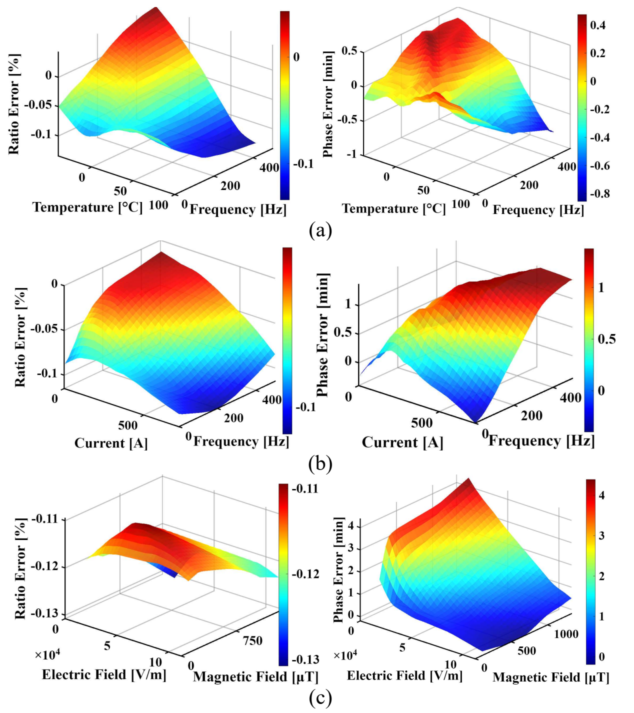

Fig. 9. Error prediction using CT-ErrorNet, (a) temperature vs. frequency, (b) current vs. frequency, (c) electric field vs. magnetic field.

TABLE I. COMPARATIVE EXPERIMENT FOR DIFFERENT METHODS

Test Points	Methods (Ratio/phase Error)		
	Polynomial Regression (%)	CT-ErrorNet (%)	Benchmark (%)
1(50A, 10Hz)	-0.0638/0.05	-0.0607/0.06	-0.0598/0.061
2(60A, 40°C)	-0.066/0.02	-0.0613/0.058	-0.059/0.0472
3(100A, 100Hz)	-0.0618/-0.01	-0.0524/0.052	-0.0515/0.0376
RMSE	0.02344%	0.007437%	-
Testing time	7.62s	9.16s	654s

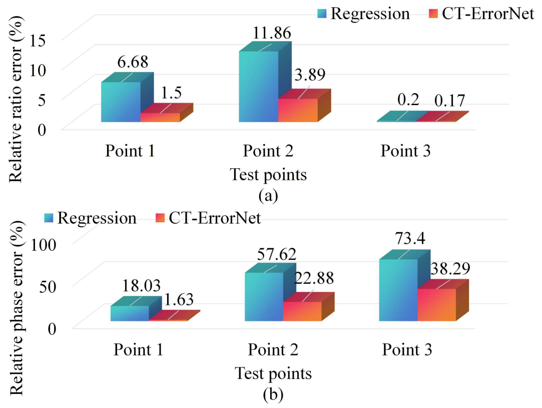

Fig. 10. Relative ratio and phase errors.

demonstrating a transformative improvement in computational efficiency.

V. CONCLUSION

To address the myriad factors influencing current transformer error and to enhance simulation efficiency, this paper examines metering current transformers under multiple external influences and proposes CT-ErrorNet for error prediction under limited test conditions. The considered factors include primary current amplitude, frequency, temperature, and electromagnetic fields. Through theoretical analysis and finite element-based simulations, the following results are established: the ratio error first decreases and then increases with increasing current amplitude; decreases and eventually stabilizes with increasing frequency; increases with both temperature and magnetic flux density; and is largely insensitive to electric field intensity. The phase error generally increases with current amplitude; initially increases and then decreases with frequency; and increases with both temperature and magnetic flux density, while likewise exhibiting negligible sensitivity to electric field intensity. Based on these insights, the proposed CT-ErrorNet achieves threefold lower relative ratio and phase errors compared to the Polynomial Regression, significantly enhances simulation efficiency under limited test conditions, and reduces the computational time cost by over 70 times compared to the benchmark.

REFERENCES

[1] Z. Zhang, J. Wu, K. Li, and L. Ding, "Detection method for current transformer metering error of high-voltage line group based on hierarchical progression," *IEEE Trans. Instrum. Meas.*, vol. 74, pp. 1-10, 2025, Art. no. 1014010.

[2] L. Chen, "Influence of current transformer on electric energy measurement," *Power Autom. Equip.*, vol. 31, no. 1, pp. 138-141, 2011.

[3] Y. Wang, Q. Tang, J. Ma, W. Qiu, and Y. Yang, "Basic error prediction method of smart meter based on compound kernel SVM," *J. Electron. Meas. Instrum.*, vol. 35, no. 10, pp. 209-216, 2021.

[4] J. Zhang, J. Xiao, N. Liu, S. Tan, and W. Li, "Research on the error analysis of electric energy metering devices in AC power transmission systems," in *Proc. 6th Asia Energy Electr. Eng. Symp. (AEEES)*, Chengdu, China, 2024, pp. 88-92.

[5] IEEE Draft Guide for the Synchronous Monitoring of Direct Current (DC) Bias Magnetic Current Distribution in Power Grid, IEEE Std. P2869/D7, Apr. 27, 2021.

[6] C. He, X. Xia, B. Zhang, W. Kang, J. Zhang, and H. Chen, "Analyzing adjustment and verification errors in electric metering devices for smart power systems considering multiple environmental factors," *AIP Adv.*, vol. 14, no. 12, 2024, Art. no. 125324.

[7] Y. Qin, W. Qiu, Y. Luo, R. Tang, K. Sun, and H. Yin, "Degradation analysis: Modeling and evaluating for electric energy meters under multistress," *IEEE Trans. Ind. Informat.*, vol. 21, no. 9, pp. 6615-6625, Sep. 2025.

[8] T. Biswas, S. De, and A. Basuray, "Analysis and discrimination of transformer inrush current and fault current," in *Proc. IEEE 7th Int. Conf. Cond. Assessment Techn. Electr. Syst. (CATCON)*, Kolkata, India, 2024, pp. 249-254.

[9] Q. Zhang, M. Liu, W. Zhang, and B. Wu, "Research on frequency characteristics of errors in low-voltage current transformers," in *Proc. IEEE 7th Int. Electr. Energy Conf. (CIEEC)*, Harbin, China, 2024, pp. 372-377.

[10] T. Li, Q. Chen, X. Zhang, and H. Lu, "Analysis of the influence of ambient temperature on the optical fiber characteristics of fiber optic current transformer sensor," in *Proc. IEEE 7th Int. Electr. Energy Conf. (CIEEC)*, Harbin, China, 2024, pp. 1692-1696.

[11] N. Ivanov, R. Kanafeev, and V. Terzija, "Impact of electromagnetic and optical CTs on transformer differential protection during transformer re-energization," in *Proc. IEEE Belgrade PowerTech*, Belgrade, Serbia, 2023, pp. 1-6.

[12] C. Lei and L. He, "Analysis of the electric field at the tip of the converter transformer under the influence of temperature gradient," in *Proc. 6th Int. Conf. Electr. Eng. Control Technol. (CEECT)*, Shenzhen, China, 2024, pp. 279-283.

979-8-3315-8138-1